processes

MDPI

Article

Physics-Informed Neural Networks for Parameter Identification of Equivalent Thermal Parameters in Residential Buildings During Winter Electric Heating

Sijia Liu *, Qi An, Ziyi Yuan and Pengchao Lei

College of Automation, Beijing Information Science and Technology University, Beijing 100192, China; 2023020422@bistu.edu.cn (Q.A.); ziyi_yuan011@163.com (Z.Y.); 2024020505@bistu.edu.cn (P.L.)
* Correspondence: sjliu@bistu.edu.cn

Abstract

Accurate identification of equivalent thermal parameters (ETPs) is crucial for optimizing energy efficiency in residential buildings during winter electric heating. This study proposes a physics-informed neural network (PINN) approach to estimate ETP model parameters, integrating physical constraints with data-driven learning to enhance robustness. The method is validated using real-world measurements from seven rural residences, with indoor and outdoor temperatures and heating power sampled every 15 min. The PINN is compared with linear regression (LR), heuristic methods (GA, PSO, TROA), and data-driven methods (RF, XGBoost, LSTM). The results show that the PINN reduces MAE by over 90% compared to LR, 42% compared to heuristic methods, and 75% compared to pure data-driven methods, with similar improvements in RMSE and MAPE, while maintaining moderate computational time. This work highlights the potential of PINNs as an efficient and reliable tool for building energy management, offering a promising solution for parameter identification within the specific context of the studied residences, with future work needed to confirm scalability across diverse climates and building types.

Keywords: PINN; ETP; parameter identification; thermal dynamics modeling; winter electric heating; real-world data validation

check for updates

Academic Editors: Qianyi Liu and Jiayan Liu

Received: 18 August 2025
Revised: 1 September 2025
Accepted: 5 September 2025
Published: 7 September 2025

Citation: Liu, S.; An, Q.; Yuan, Z.; Lei, P. Physics-Informed Neural Networks for Parameter Identification of Equivalent Thermal Parameters in Residential Buildings During Winter Electric Heating. *Processes* **2025**, *13*, 2860. https://doi.org/10.3390/pr13092860

Copyright: © 2025 by the authors. Licensee MDPI, Basel, Switzerland. This article is an open access article distributed under the terms and conditions of the Creative Commons Attribution (CC BY) license (https://creativecommons.org/licenses/by/4.0/).

1. Introduction

In recent years, due to growing environmental concerns, an increasing number of rural residences have adopted electric heating to replace traditional heating methods, reducing carbon emissions and improving sustainability [1,2]. This transition to electric heating offers residents more comfortable and controllable warming with lower pollution, but it significantly impacts power system loads, causing increased peak demand, grid instability, and higher operational costs [3,4]. To effectively regulate residential heating loads, dynamic modeling of building thermo-electric dynamics is essential, with the *thermal parameter* (ETP) model being a widely adopted approach for simulating heat transfer and storage in residential buildings [5,6]. However, accurate identification of ETPs, such as thermal resistances and capacitances, is critical for optimizing building energy management, yet challenges persist due to data noise, system uncertainties, complex non-linear dynamics (e.g., non-linear heat transfer due to varying insulation), computational efficiency, and robustness [7,8]. ETP identification primarily encompasses three categories: *statistical methods*, *heuristic optimization techniques*, and *pure data-driven approaches*, each with distinct strengths and limitations.

Statistical methods, such as multiple regression and least-squares approaches, are widely adopted to estimate ETPs from real-world data [9–13]. For instance, multiple regression models achieve high correlation in controlled settings but struggle with intricate parameter interactions and data noise, necessitating extensive calibration [9,10]. These approaches, while computationally simple, lack scalability for complex building scenarios [13].

Heuristic optimization methods, including Genetic Algorithms (GAs), Particle Swarm Optimization (PSO), and the Tyrannosaurus Rex Optimization Algorithm (TROA), enhance global search capabilities for ETP estimation [14–18]. These techniques improve convergence in diverse datasets, such as through improved Harris Hawk optimization for air conditioning loads [18]. However, they are computationally expensive and remain sensitive to initial conditions, limiting practical application [19,20].

Pure data-driven methods, such as Random Forest (RF), XGBoost, and Long-Short Term Memory (LSTM), model complex behaviors in building thermal dynamics, offering flexibility in handling uncertainties [21–23]. However, these methods produce black-box mappings lacking physical interpretability; for instance, in ETP identification, they predict indoor temperatures from historical data but cannot estimate thermal resistances or capacitances; moreover, they require large datasets to avoid overfitting, reducing robustness with limited or noisy data [24].

In summary, these methods face challenges in computational efficiency, robustness to noise, and physical interpretability, particularly in scenarios with limited data or complex dynamics. Statistical methods lack scalability, heuristic optimizations are computationally intensive, and data-driven approaches fail to provide interpretable parameters, hindering their applicability in energy management.

Physics-informed neural networks (PINNs) address these issues by integrating physical constraints via physical loss into the learning process, enhancing robustness and enabling it to capture the physical dynamics even in scenarios absent from training data [25]. PINNs are suitable for inverse problems; meanwhile, the ETP identification is a typical inverse problem, and PINNs effectively tackle such challenges by embedding governing equations (ETP model) into the loss function. For instance, ref. [26] applied a PINN to identify the parameters of a first-order ETP model using simulated data, validating its effectiveness against linear regression.

This study applies a PINN to identify the parameters of a second-order ETP model, closer to real building thermal dynamics. The proposed framework leverages real-world operational data from seven rural residences for validation, comparing the PINN with statistical (linear regression), heuristic (GA, PSO, and TROA), and data-driven (RF, XGBoost, and LSTM) methods, to demonstrate superior accuracy and efficiency. By embedding physical constraints into the neural network, the PINN uniquely combines data-driven flexibility with physical interpretability, offering a robust solution for ETP identification in complex building scenarios.

The remainder of the paper is organized as follows: Section 2 details the methodology, including the ETP model and PINN framework; Section 3 evaluates the methods using data from seven rural residences; Section 4 discusses the results and limitations; and Section 5 concludes the study with future research directions.

2. Methods

2.1. Equivalent Thermal Parameters (ETPs) Model

The *Equivalent Thermal Parameters* (ETPs) model provides a simplified yet effective approach for simulating building thermal dynamics, widely applied in energy management and load forecasting for residential buildings [27]. By employing an analogy to electrical

circuits, the model represents heat transfer through thermal resistances (R) and heat storage through thermal capacitances (C), facilitating the prediction of indoor temperature variations under external conditions such as outdoor temperature and heating inputs. This approach is particularly suitable for optimizing demand response strategies in winter electric heating scenarios.

In this study, a second-order ETP model (illustrated in Figure 1) is adopted, comprising two coupled differential equations that describe the dynamics of indoor air temperature (T_i) and indoor solid temperature (T_s, including walls, ceiling, and floor). It describes the thermal dynamics of buildings, using two coupled differential equations, as shown in Equation (1):

$$\begin{cases} C_1 \dfrac{dT_i}{dt} = \dfrac{T_o - T_i}{R_1} + \dfrac{T_s - T_i}{R_2} + Q \\ C_2 \dfrac{dT_s}{dt} = \dfrac{T_i - T_s}{R_2} \end{cases} \tag{1}$$

where T_o denotes the outdoor temperature (°C), $Q = \eta P$ is the heat input (kW) with η as the electric heater efficiency converting electric power P(kW) to heat, R_1 is the thermal resistance (°C/kW) between outdoor and indoor air, R_2 is the thermal resistance (°C/kW) between indoor air and indoor solid temper, and C_1 and C_2 are thermal capacitances (kWh/°C) for indoor air and indoor solid, respectively. The model assumes steady-state heat flow, negligible radiative heat transfer, and constant parameters, which are reasonable for short-term simulations in controlled environments.

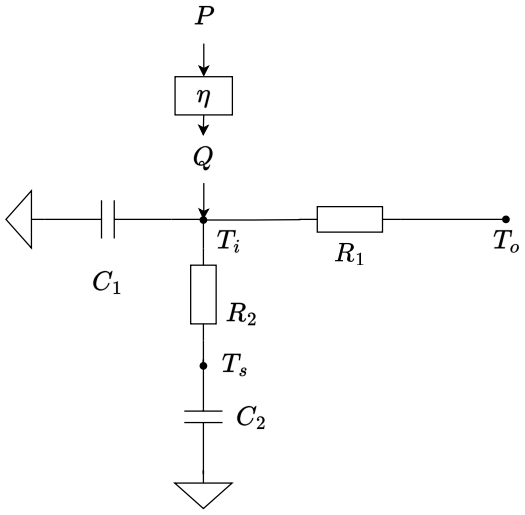

Figure 1. Schematic of the second-order ETP model.

These equations effectively capture the heat balance in buildings, enabling accurate temperature response predictions. However, identifying the parameters (R_1, R_2, C_1, C_2) from operational data remains challenging due to complex dynamics and data noise, motivating the use of advanced methods like physics-informed neural networks, as discussed in the subsequent sections.

2.2. Physics-Informed Neural Network (PINN) Method

Physics-informed neural networks (PINNs) represent a powerful computational paradigm that integrates data-driven machine learning with physical laws, offering a robust framework for solving forward and inverse problems in scientific computing [25]. Unlike conventional neural networks, which rely solely on observational data, PINNs embed governing physical equations directly into the learning process, ensuring that predictions adhere to underlying principles. This hybrid approach enhances generalization,

particularly in scenarios with limited data or complex systems, making PINNs well-suited for applications requiring high accuracy and interpretability.

The PINN framework employs a deep neural network to approximate solutions to physical systems. The network typically consists of multiple hidden layers with non-linear activation functions, taking independent variables (e.g., time and environmental inputs) as inputs and outputting dependent variables (e.g., system states). The training process minimizes a composite loss function defined as:

$$\mathcal{L} = \mathcal{L}_{\text{data}} + \lambda \mathcal{L}_{\text{physics}} \tag{2}$$

where $\mathcal{L}_{\text{data}}$ measures the difference between predicted and observed data (e.g., mean squared error), $\mathcal{L}_{\text{physics}}$ enforces physical constraints by minimizing residuals of governing equations, and λ is a weighting factor balancing data accuracy and physical consistency. Automatic differentiation computes derivatives required for physical residuals, enabling efficient integration of differential equations. The training objective (Equation (3)) ensures convergence by driving the gradient norm of the loss function to zero, optimizing parameters to satisfy both data and physical constraints.

$$\|\nabla \mathcal{L}\| \to 0 \tag{3}$$

The PINN's ability to incorporate physical knowledge makes it a promising tool for parameter identification in complex systems, such as ETP models for building thermal dynamics, as detailed in the subsequent section.

2.3. PINN-Based Parameter Identification for ETP Models

In this paper, we apply the PINN framework to identify parameters of the second-order ETP model, including thermal resistances (R_1, R_2) and capacitances (C_1, C_2), through a hybrid loss function. The following sections outline the implementation steps, including data preprocessing, network configuration, and optimization.

First, data preprocessing ensures numerical stability and model performance. The dataset, comprising time (t), outdoor temperature (T_o), heating power (P), and indoor temperature (T_i), is first divided into 80% for training and lastly 20% for testing. Missing values in the real-world measurements were filled via linear interpolation, and variables were normalized to [0, 1] using Equation (4) to ensure numerical stability during training; no additional denoising techniques were applied, as PINN's physics-informed constraints (Equation (6)) enhance robustness to measurement noise.

$$x_{\text{norm}} = \frac{x - x_{\min}}{x_{\max} - x_{\min}} \tag{4}$$

Second, the PINN is configured as a feed-forward neural network with non-linear activation functions, taking normalized inputs (t, T_o, P) and outputting predicted states (T_i, T_s). The loss function, as defined in Equation (2), combines data loss and physics loss. The data loss shown in (5) is the mean squared error:

$$\mathcal{L}_{\text{data}} = \frac{1}{N} \sum_{i=1}^{N} \left(T_i^{\text{pred}} - T_i^{\text{obs}} \right) \tag{5}$$

The physics loss minimizes residuals of the ETP equations (Equation (6)):

$$\mathcal{L}_{\text{physics}} = \frac{1}{N} \left(res_1^2 + res_2^2 \right) \tag{6}$$

where

$$res_1 = C_1 \frac{\mathrm{d}T_i^{\mathrm{pred}}}{\mathrm{d}t} - \frac{T_o - T_i^{\mathrm{pred}}}{R_1} - \frac{T_s^{\mathrm{pred}} - T_i^{\mathrm{pred}}}{R_2} - Q \tag{7}$$

$$res_2 = C_2 \frac{\mathrm{d}T_s^{\mathrm{pred}}}{\mathrm{d}t} - \frac{T_i^{\mathrm{pred}} - T_s^{\mathrm{pred}}}{R_2} \tag{8}$$

Automatic differentiation computes derivatives for the residuals in Equations (7) and (8), ensuring physical consistency during training.

Finally, the optimization process minimizes the total loss (Equation (2)) to estimate R_1, R_2, C_1, and C_2, generating T_i^{pred} by inputting P and T_o into the PINN, with convergence monitored via Equation (3). A multi-initial value strategy performs 10 initializations with parameters (R_1, R_2 in [1, 10] °C/kW, C_1, C_2 in [0.1, 10] kWh/°C) sampled randomly without fixed seeds to explore diverse starting points, selecting the parameter set with the lowest total loss across runs. Convergence stability is ensured by early stopping when the loss change falls below $\epsilon_{\mathrm{stop}} = 10^{-5}$, preventing overfitting and ensuring robust parameter estimation. The training process is detailed in Algorithm 1.

Algorithm 1: PINN Training for Parameter Identification

Require: Training data: t, T_o, P, T_i^{obs}; Initial parameters; Hyperparameters: λ, max iterations, learning rate, ϵ_{stop}// `ϵstop denotes the threshold for early stopping to prevent overfitting`

Ensure: Optimized parameters: R_1, R_2, C_1, C_2

```
Initialize PINN network and parameters
for iteration = 1 to max iterations do
    Compute predicted states T_i^pred, T_s^pred
    Calculate data loss using MSE
    Compute derivatives via automatic differentiation
    Calculate physics residuals (Equation (1))
    Compute total loss (Equation (2))
    Backpropagate and update parameters
    if loss change < ϵ_stop then
        Break
    end if
end for
return Optimized parameters
```

3. Case Study

3.1. Dataset Description

This case study utilizes a dataset collected from seven rural residences in northern China (ten residences were initially measured, but only six collected complete data (1056 points each); one residence had up to one day of data loss (970 points retained), while three were excluded due to over 60% data loss, including one with no data), sampled at 15 min intervals over 11 days in December 2023, yielding up to 1056 data points per residence.The dataset was utilized individually to train models for each residence. The 11-day period was selected to capture a representative range of winter weather conditions, including temperature fluctuations and typical heating patterns, while ensuring data continuity and equipment reliability during the measurement campaign. The dataset comprises timestamps (t, 15 min intervals), indoor air temperature (T_i, °C), outdoor temperature (T_o, °C), and heating power (P, kW). Indoor temperatures were measured directly within the residences, while outdoor temperatures, identical across all residences, were obtained

from a local meteorological station. Heating power was recorded by electric heater monitoring devices. Power data were sampled every 15 min, whereas temperature data (T_i, T_o) were recorded hourly and interpolated to 15 min intervals using spline interpolation, chosen for its smoothness in capturing continuous temperature variations, which is suitable for the gradual changes in real-world temperature data. The spline interpolation of may introduce autocorrelation, but this affects all methods equally, ensuring fair comparisons. Figure 2 illustrates the interpolated 15 min outdoor temperature profile from the meteorological station, showing daily variations in winter conditions.

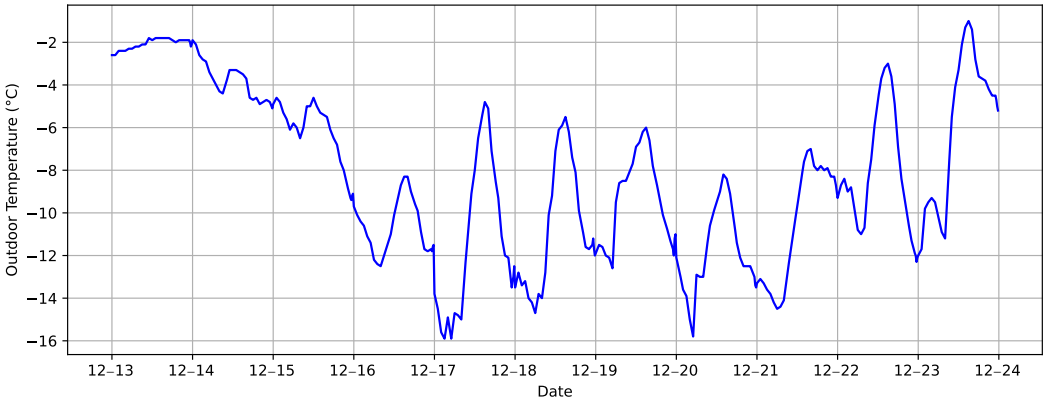

Figure 2. Outdoor temperature profile (15 min interpolated data) from meteorological station.

3.2. Objectives and Validation Methods

The PINN framework is compared with linear regression, heuristic optimization methods (GA, PSO, TROA), and data-driven methods (RF, XGBoost, LSTM) for identifying parameters of the second-order ETP model. Since actual thermal parameters are unavailable, validation focuses on comparing predicted indoor temperatures (T_i^{pred}) with observed values (T_i^{obs}) on the test set (20%, last 212 points). Parameter-based methods (PINN, LR, GA, PSO, TROA) generate T_i^{pred} by inputting test set operational data (P, T_o) into their respective models, while data-driven methods directly predict T_i^{pred}. Errors are quantified using mean absolute error (MAE), root mean square error (RMSE), and mean absolute percentage error (MAPE), defined as in Equation (9):

$$\begin{cases} \text{MAE} = \dfrac{1}{N}\displaystyle\sum_{i=1}^{N} |T_i^{\text{pred}} - T_i^{\text{obs}}|, \\ \text{RMSE} = \sqrt{\dfrac{1}{N}\displaystyle\sum_{i=1}^{N} (T_i^{\text{pred}} - T_i^{\text{obs}})^2}, \\ \text{MAPE} = \dfrac{100}{N}\displaystyle\sum_{i=1}^{N} \left| \dfrac{T_i^{\text{pred}} - T_i^{\text{obs}}}{T_i^{\text{obs}} + eps} \right|, \end{cases} \tag{9}$$

where *eps* prevents division by zero. Computational efficiency is assessed via training time per residence.

3.3. Simulation Environment

The experiments were conducted on a computing platform with an `Intel Core i5-11400F` CPU, `NVIDIA RTX 2060 Super` GPU, and `32 GB 3200 MHz` memory. The operating system was `Windows 11 24H2`. Software implementations utilized `Python 3.10.6`, with key libraries including `PyTorch 2.6.0`, `scikit-learn 1.6.1`, and `xgboost 3.0.1`.

3.4. Experimental Setup and Results

3.4.1. Experimental Setup

The experiments were conducted using the dataset and environment described in Sections 3.1 and 3.3. The PINN framework, implemented as a feed-forward neural network with 3–5 layers and Tanh activation, uses a learning rate of 0.001, $\lambda = 1$, and early stopping threshold $\epsilon_{\text{stop}} = 10^{-5}$, as detailed in Algorithm 1. Physics residuals are enforced at the observed training timestamps (844 points) to compute the physical loss term in the PINN framework. PINN hyperparameters, including the physics loss weight $\lambda = 1$, were empirically selected based on standard practices in neural network training, commonly used for similar scientific computing tasks to balance data and physics losses. No additional denoising, regularization, or Bayesian uncertainty quantification techniques were applied, as PINN's physics-informed constraints inherently mitigate the impact of noise in real-world data. LR employs a second-order ETP model with least-squares fitting. GA, PSO, and TROA, implemented via custom programming, optimize parameters (R_1, R_2, C_1, C_2) with a population size of 50 and 1000 iterations, initializing parameters within physical ranges (e.g., $R_1 \in [1, 10]$ K/kW). RF uses 100 trees, XGBoost uses a learning rate of 0.1 and 100 trees, and LSTM uses two layers with 50 hidden units, trained on 80% of the data (No. 1–844 points) and tested on 20% (No. 845– 1056 points). All methods were evaluated using MAE, RMSE, and MAPE (Equation (9)) on the test set, with computational efficiency measured by training time per residence. Table 1 summarizes the hyperparameter settings.

Table 1. Hyperparameter settings for compared methods.

Method	Hyperparameters
PINN	Layers: 3–5, tanh activation, learning rate 0.001, physical weight: 1, $\epsilon_{\text{stop}} = 10^{-5}$
LR	Least-squares fitting, second-order ETP model
GA	Population: 50, Iter: 1000, Init search space: $R_1, R_2 \in [1, 10]$, $C_1, C_2 \in [0.1, 10]$
PSO	Population: 50, Iter: 1000, Init search space: $R_1, R_2 \in [1, 10]$, $C_1, C_2 \in [0.1, 10]$
TROA	Population: 50, Iter: 1000, Init search space: $R_1, R_2 \in [1, 10]$, $C_1, C_2 \in [0.1, 10]$
RF	Trees: 100, Max depth: 10
XGBoost	Learning rate: 0.1, Trees: 100
LSTM	Layers: 2, Hidden units: 50, Learning rate: 0.001

3.4.2. Results and Efficiency Analysis

The PINN, LR, GA, PSO, and TROA methods generate predicted indoor temperatures (T_i^{pred}) by inputting test set operational data (P, T_o, 212 points) into their respective models. RF, XGBoost, and LSTM directly predict T_i^{pred} using the test set. Prediction accuracy is evaluated using MAE, RMSE, and MAPE (Equation (9)). Table 2 presents the average error metrics and 95% confidence intervals across seven residences, calculated using the t-distribution with a critical value $t_{0.025,6} \approx 2.447$. The high MAPE values for RF, XGBoost, and LSTM are primarily due to large prediction deviations in Room 1 under the non-training conditions specialized in Section 4. Figure 3 shows boxplots of MAE, RMSE, and MAPE distributions across the seven residences, highlighting PINN's consistently low errors and small variance. Figure 4 provides a detailed comparison of predicted vs. observed indoor temperatures for a representative residence, demonstrating PINN's alignment with observed data.

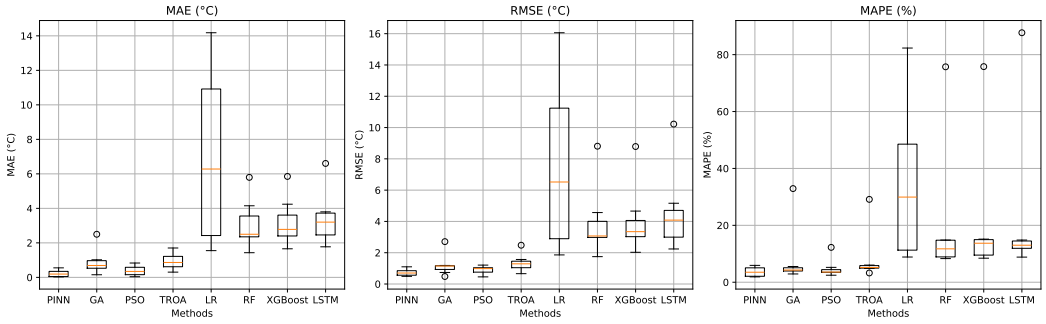

Figure 3. Boxplots of MAE, RMSE, and MAPE distributions across seven residences for compared methods.

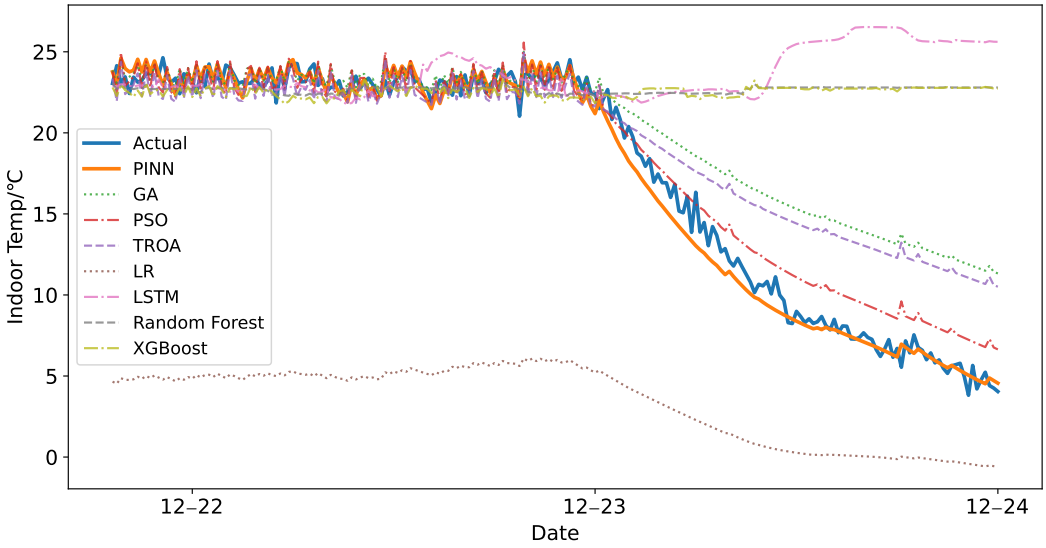

Figure 4. Predicted vs. observed indoor temperature for one of the representative residences. The heater in this house is manually turned off after 12–23, scenarios absent from training data.

Table 2. Error metrics (averaged over seven residences).

Method	MAE (°C)	RMSE (°C)	MAPE (%)
PINN	0.223 ± 0.191 [0.05, 0.40]	0.73 ± 0.20 [0.54, 0.92]	3.66 ± 1.57 [2.21, 5.11]
LR	6.957 ± 4.863 [2.46, 11.46]	7.53 ± 5.13 [2.79, 12.27]	34.39 ± 26.97 [9.46, 59.32]
GA	0.905 ± 0.656 [0.35, 1.47]	1.22 ± 0.70 [0.62, 1.82]	8.31 ± 10.07 [0.74, 15.88]
PSO	0.385 ± 0.242 [0.19, 0.58]	0.89 ± 0.28 [0.66, 1.12]	4.88 ± 3.10 [2.27, 7.49]
TROA	0.934 ± 0.468 [0.57, 1.30]	1.35 ± 0.54 [0.91, 1.79]	8.45 ± 8.48 [2.36, 14.54]
RF	3.077 ± 1.345 [1.98, 4.18]	3.94 ± 2.13 [2.28, 5.60]	20.45 ± 22.71 [3.39, 37.51]
XGBoost	3.187 ± 1.309 [2.11, 4.26]	4.05 ± 2.07 [2.44, 5.66]	20.99 ± 22.52 [3.99, 37.99]
LSTM	3.421 ± 1.462 [2.24, 4.60]	4.56 ± 2.48 [2.68, 6.45]	23.20 ± 26.40 [1.41, 44.99]

Computational efficiency was assessed by training time per residence, as shown in Table 3. PINN requires 14.594 s, although not the least, balancing superior accuracy with moderate computational cost. LSTM is slower due to sequential processing, while heuristic methods are computationally intensive due to iterative optimization. PINN's efficiency, combined with its lowest prediction errors, underscores its practical advantage for ETP identification. Computational times in Table 3 were obtained on the CPU (Intel Core i5-11400F) for all methods, as initial GPU tests showed no advantage due to the small dataset size (844 training points) and data transfer overhead. PINN and LSTM used early stopping, typically converging within 2500–3000 (5000 max) and 350–600 (1000 max) epochs,

respectively. GA, PSO, and TROA used 1000 iterations, LR used a single fit, and RF and XGBoost used 100 trees.

Table 3. Computational time per residence (seconds).

Method	PINN	LR	GA	PSO	TROA	RF	XGBoost	LSTM
Time (s)	14.6 ± 0.9	0.24 ± 0.03	1165.5 ± 79	451.4 ± 21.6	226.3 ± 24.3	0.24 ± 0.01	0.041 ± 0.003	71.2 ± 3.6

4. Discussion

Section 3 presents the results of the PINN method compared to statistical (LR), heuristic (GA, PSO, TROA), and data-driven (RF, XGBoost, LSTM) methods for house ETP identification. Table 2 demonstrates PINN's superior performance, achieving the lowest MAE (0.731 ± 0.204 °C), RMSE (0.223 ± 0.191 °C), and MAPE (3.662 ± 1.570%) by integrating physical constraints into the neural network, which enhances accuracy and robustness even with limited or noisy data. Compared to recent PINN applications [26], our approach leverages the ETP model (Equation (1)) for building thermal dynamics, achieving high accuracy in parameter identification with simpler physical constraints, demonstrating its suitability for practical energy management. From these results, it can be seen that the PINN method has the following advantages:

The PINN method can capture physical laws. Figure 4 shows the temperature curve corresponding to the test set for one of the seven rooms in the case study, with the heater power shown in Figure 5. From the heater power curve, it can be seen that for most of the time on the last day of testing, the room's heater power was 0, causing a continuous decline in room temperature (possibly due to the room residents being out that day, leading to all power being turned off). This situation did not occur in the training set; although there were a few instances of heater power being 0 in the training set, the duration was short, and the indoor temperature did not drop very low. Therefore, machine learning-based methods (RF, XGBoost, LSTM) cannot capture this anomalous scenario, resulting in significant deviations in their predictions. In contrast, the PINN method captures the physical law between heater power and indoor temperature, achieving success even in data patterns absent from the training set. From another perspective, it can also be said that the PINN method overcomes, to some extent, the **lack of interpretability** in traditional deep learning models.

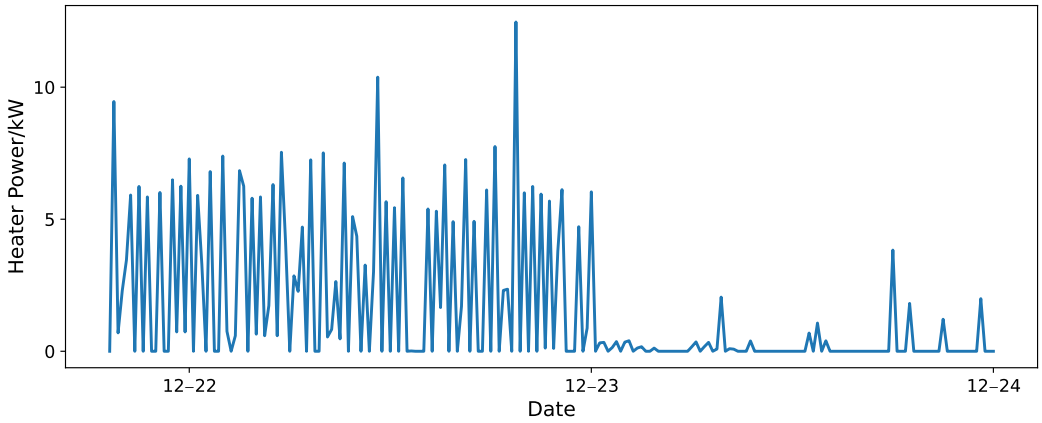

Figure 5. The heater power of the representative residence.

The PINN method exhibits good robustness. From the previous results, it can be seen that the PINN method not only has smaller errors but also smaller variations across different cases, demonstrating good robustness, while other methods show large differences in errors across different cases, making the PINN method more suitable for practical

applications. Notably, PINN achieves this robust performance without extensive hyperparameter optimization, relying on empirically selected parameters, which underscores its practical applicability. Of course, it should be noted that the robustness of the PINN method is related to the embedded physical model. The choice of the physics loss weight $\lambda = 1$ balances data fidelity and physical consistency, but its impact on convergence and accuracy warrants further exploration through sensitivity analysis in future work.

It should be pointed out that the physical model studied in this paper (ETP), designed with constant parameters, has relatively simple dynamic performance, and does not account for dynamic processes such as radiation, internal gains, or infiltration variations, which may bias parameter recovery. This simplification supports the study's focus on efficient identification, though future work will explore these effects through time-varying parameter modeling.

5. Conclusions

This study proposed a PINN framework for identifying parameters of the second-order ETP model in building thermal dynamics. The framework integrates physical constraints into the learning process, enabling robust parameter estimation from operational data. The methodology was validated using real-world measurements from seven rural residences, comparing PINN with linear regression (LR), heuristic optimization methods (GA, PSO, TROA), and data-driven approaches (RF, XGBoost, LSTM). The results showed PINN's superior performance in prediction accuracy and robustness, as evidenced by low errors and variance across cases. The research significance lies in providing a hybrid method that combines data-driven flexibility with physical interpretability, advancing building energy management within the context of the studied dataset. The research significance lies in providing a hybrid method that combines data-driven flexibility with physical interpretability, advancing building energy management and demand response applications.

Future work could focus on validating the PINN framework across diverse climates, building types, and insulation qualities to confirm its scalability. Additionally, optimizing PINN's computational efficiency through advanced techniques like parallel processing or model compression. Additionally, extending the framework to more complex building models with non-linear dynamics would further enhance its applicability. Future research could also explore Bayesian uncertainty quantification to further address data noise and improve parameter estimation reliability. Furthermore, experiments with typical houses, where architectural standards provide accurate parameter benchmarks, will be conducted to validate parameter estimates, uncertainty, and identifiability.

Author Contributions: Conceptualization, S.L.; data curation, Q.A., Z.Y. and P.L.; methodology, S.L.; validation, S.L. and Q.A.; visualization, Q.A., Z.Y. and P.L.; writing—original draft, S.L. All authors have read and agreed to the published version of the manuscript.

Funding: This research received no external funding.

Institutional Review Board Statement: Not applicable.

Data Availability Statement: The original contributions presented in this study are included in the article. Further inquiries can be directed to the corresponding author.

Conflicts of Interest: The authors declare no conflicts of interest.

References

1. Shi, Q.; Li, F.; Hu, Q.; Wang, Z. Dynamic demand control for system frequency regulation: Concept review, algorithm comparison, and future vision. *Electr. Power Syst. Res.* **2018**, *154*, 75–87. [CrossRef]
2. Bastida, H.; Ugalde-Loo, C.E.; Abeysekera, M.; Qadrdan, M.; Wu, J. Thermal Dynamic Modelling and Temperature Controller Design for a House. *Energy Procedia* **2019**, *158*, 2800–2805. [CrossRef]
3. Lu, N. An Evaluation of the HVAC Load Potential for Providing Load Balancing Service. *IEEE Trans. Smart Grid* **2012**, *3*, 1263–1270. [CrossRef]
4. Zhang, L.; Liu, X.; Zhang, J. Regulation capability evaluation of individual electric heating load based on radial basis function neural network. *Therm. Sci.* **2019**, *23*, 2821–2829. [CrossRef]
5. Amadeh, A.; Lee, Z.E.; Max Zhang, K. Building cluster demand flexibility: An innovative characterization framework and applications at the planning and operational levels. *Energy Convers. Manag.* **2023**, *283*, 116884. [CrossRef]
6. Cheng, L.M.; Bao, Y.Q. A Day-Ahead Scheduling of Large-Scale Thermostatically Controlled Loads Model Considering Second-Order Equivalent Thermal Parameters Model. *IEEE Access* **2020**, *8*,102321–102334. [CrossRef]
7. Reynolds, A. Liberating Lévy walk research from the shackles of optimal foraging. *Phys. Life Rev.* **2015**, *14*, 59–83. [CrossRef]
8. Li, Y.; O'Neill, Z.; Zhang, L.; Chen, J.; Im, P.; DeGraw, J. Grey-box modeling and application for building energy simulations—A critical review. *Renew. Sustain. Energy Rev.* **2021**, *146*, 111174. [CrossRef]
9. Pokorska-Silva, I.; Nowoświat, A.; Fedorowicz, L. Identification of thermal parameters of a building envelope based on the cooling process of a building object. *J. Build. Phys.* **2020**, *43*, 503–527. [CrossRef]
10. Wang, J.; Jiang, Y.; Tang, C.Y.; Song, L. Development and validation of a second-order thermal network model for residential buildings. *Appl. Energy* **2022**, *306*, 118124. [CrossRef]
11. Rivera, A.K.; Sánchez, J.; Chen Austin, M. Parameter identification approach to represent building thermal dynamics reducing tuning time of control system gains: A case study in a tropical climate. *Front. Built Environ.* **2022**, *8*, 949426. [CrossRef]
12. De Coninck, R.; Magnusson, F.; Åkesson, J.; Helsen, L. Toolbox for development and validation of grey-box building models for forecasting and control. *J. Build. Perform. Simul.* **2016**, *9*, 288–303. [CrossRef]
13. Shamsi, M.H.; Ali, U.; Mangina, E.; O'Donnell, J. Feature assessment frameworks to evaluate reduced-order grey-box building energy models. *Appl. Energy* **2021**, *298*, 117174. [CrossRef]
14. Bao, Y.; Cheng, L. Parameter Identification Method of Second-order Equivalent Thermal Parameter Model for Air Conditioning Loads. *Dianli Xitong Zidonghua/Autom. Electr. Power Syst.* **2021**, *45*, 37–43. [CrossRef]
15. Wu, C.; Shen, H.; Wang, Z.; Huang, T.; Fan, S.; He, G. Data-driven Online Identification Method for Parameters of Inverter Air-conditioning Load Model. *Dianli Xitong Zidonghua/Autom. Electr. Power Syst.* **2022**, *46*, 120–129. [CrossRef]
16. Sahu, V.S.D.M.; Samal, P.; Panigrahi, C.K. Tyrannosaurus optimization algorithm: A new nature-inspired meta-heuristic algorithm for solving optimal control problems. *E-Prime-Adv. Electr. Eng. Electron. Energy* **2023**, *5*, 100243. [CrossRef]
17. Zhang, S.; Shi, H.; Wang, B.; Ma, C.; Li, Q. A Dynamic Hierarchical Improved Tyrannosaurus Optimization Algorithm with Hybrid Topology Structure. *Mathematics* **2024**, *12*, 1459. [CrossRef]
18. Wu, K.; Yu, Y. Parameter Identification Method for Air Conditioning Load Models Based on Improved Harris Hawk Optimization Algorithm. In Proceedings of the 7th IEEE International Conference on Information Systems and Computer Aided Education (ICISCAE 2024), Dalian, China, 27–29 September 2024; pp. 783–790. [CrossRef]
19. Leprince, J.; Madsen, H.; Miller, C.; Real, J.P.; van der Vlist, R.; Basu, K.; Zeiler, W. Fifty shades of grey: Automated stochastic model identification of building heat dynamics. *Energy Build.* **2022**, *266*, 112095. [CrossRef]
20. Rivera, A.K.; Sánchez, J.; Mora, D.; Austin, M.C. Inspection of the Identification of Thermal Modeling Process in Buildings: A Proposed Methodology for a Case Study in Tropical Climate. In *Proceedings of the Advances in Automation and Robotics Research, Monterrey, Mexico, 17–19 November 2021*; Moreno, H.A., Carrera, I.G., Ramírez-Mendoza, R.A., Baca, J., Banfield, I.A., Eds.; Springer: Cham, Switzerland, 2022; pp. 172–180. [CrossRef]
21. Song, Z.; Shi, J.; Li, S.; Chen, Z.; Jiao, F.; Yang, W.; Zhang, Z. Data-driven and physical model-based evaluation method for the achievable demand response potential of residential consumers' air conditioning loads. *Appl. Energy* **2022**, *307*, 118017. [CrossRef]
22. Guo, Z.; Coffman, A.R.; Munk, J.; Im, P.; Kuruganti, T.; Barooah, P. Aggregation and data driven identification of building thermal dynamic model and unmeasured disturbance. *Energy Build.* **2021**, *231*, 110500. [CrossRef]
23. Gao, C.; Guo, Y.; Xu, Y.; Huang, J.; Zhang, F.; Hu, W.; Liu, Q. A deep-learning approach for modeling the demand function of air conditioning resources with respect to the electricity prices. *Appl. Energy* **2025**, *392*, 125977. [CrossRef]
24. Sabir, S.; Rueda, L.; Fournier, M.; Nagarsheth, S.; Agbossou, K.; Henao, N.; Kelouwani, S. Modeling and Parameter Estimation of Electric Thermal Storage utilizing Residual Components for Residential Consumer. In Proceedings of the 2024 IEEE Conference on Technologies for Sustainability, Portland, OR, USA, 14–17 April 2024; pp. 144–150, ISSN 2640-6810. [CrossRef]
25. Raissi, M.; Perdikaris, P.; Karniadakis, G. Physics-informed neural networks: A deep learning framework for solving forward and inverse problems involving nonlinear partial differential equations. *J. Comput. Phys.* **2019**, *378*, 686–707. [CrossRef]

26. Luo, X.; Wang, Y.; Zhu, Q.; Liu, H.; Wang, S.; Wu, M. Physics-Informed Neural Network for Parameter identification of Air Conditioning Load Models. In Proceedings of the 2024 7th International Conference on Energy, Electrical and Power Engineering (CEEPE), Yangzhou, China, 26–28 April 2024; pp. 948–953. [CrossRef]
27. Sonderegger, R.C. *Dynamic Models of House Heating Based on Equivalent Thermal Parameters*; Princeton University: Princeton, NJ, USA, 1978.

Disclaimer/Publisher's Note: The statements, opinions and data contained in all publications are solely those of the individual author(s) and contributor(s) and not of MDPI and/or the editor(s). MDPI and/or the editor(s) disclaim responsibility for any injury to people or property resulting from any ideas, methods, instructions or products referred to in the content.